

# The crystal structure of ice under mesospheric conditions

Benjamin J. Murray<sup>a,\*</sup>, Tamsin L. Malkin<sup>a</sup>, Christoph G. Salzmann<sup>b</sup>

<sup>a</sup> Institute for Climate and Atmospheric Science, School of Earth and Environment, University of Leeds, Woodhouse Lane, Leeds LS2 9JT, UK

<sup>b</sup> Department of Chemistry, University College London, 20 Gordon Street, London WC1H 0AJ, UK

## ARTICLE INFO

### Article history:

Received 2 September 2014

Received in revised form

30 October 2014

Accepted 5 December 2014

Available online 10 December 2014

### Keywords:

Mesospheric clouds

Noctilucent clouds

Amorphous ice

Amorphous solid water

Stacking disordered ice

Cubic ice

## ABSTRACT

Ice clouds form in the summer high latitude mesopause region, which is the coldest part of the Earth's atmosphere. At these very low temperatures ( $< 150$  K) ice can exist in metastable forms, but the nature of these ices remains poorly understood. In this paper we show that ice which is grown at mesosphericly relevant temperatures does not have a structure corresponding to the well-known hexagonal form or the metastable cubic form. Instead, the ice which forms under mesospheric conditions is a material in which cubic and hexagonal sequences of ice are randomly arranged to produce stacking disordered ice (ice  $I_{sd}$ ). The structure of this ice is in the trigonal crystal system, rather than the cubic or hexagonal systems, and is expected to produce crystals with aspect ratios consistent with lidar observations.

© 2014 The Authors. Published by Elsevier Ltd. This is an open access article under the CC BY license (<http://creativecommons.org/licenses/by/3.0/>).

## 1. Introduction

Mesospheric ice clouds exist in a region of the Earth's atmosphere characterised by extremes of temperature and saturation. They form and exist at temperatures between 100 and 150 K where the saturation ratio commonly exceeds 100 and may occasionally reach  $10^8$  (Lübken et al., 2009). These conditions contrast with the coldest clouds in the troposphere which form at temperatures of around 185 K and with saturation ratios of less than two (Jensen et al., 2013; Wilson et al., 2012). Under these extreme conditions we need to consider the possibility that mesospheric clouds are composed of metastable forms of ice.

Water can exist as 15 crystalline phases of ice (Salzmann et al., 2011) in addition to several low temperature amorphous solid forms (Loerting et al., 2011) and high viscosity liquid phases (Palmer et al., 2014). Under mesospheric conditions the only crystalline phase thought to form is ice I (phase ice one), but ice I can exist in two well-defined structural forms: the familiar hexagonal ice (ice  $I_h$ ; ice one h), and metastable cubic ice (ice  $I_c$ ; ice one c) (Hobbs, 1974).

More recently, it has been shown that ice I has a strong propensity to exist in a state in which cubic and hexagonal sequences are interlaced to produce stacking disordered ice (Kuks et al., 2012; Malkin et al., 2015, 2012; Moore and Molinero, 2011). This material has a distinct crystal symmetry from either ice  $I_c$  and ice

$I_h$  and is referred to as ice  $I_{sd}$  (Malkin et al., 2012). In fact, it is suggested that all ice which was labelled ice  $I_c$  in the past is in fact ice  $I_{sd}$  (Hansen et al., 2008a, 2008b; Kuhs et al., 2012; Malkin et al., 2012, 2015).

In order to appreciate what stacking disorder is in the context of ice I, it is necessary to appreciate the structure of ice  $I_c$  and ice  $I_h$ . Both of these forms of ice I can be thought of as being made up of identical layers, but where the stacking of these layers differ in ice  $I_c$  and ice  $I_h$ . Each layer is made up of connected puckered six-membered rings of oxygen atoms, where the hydrogen atoms are positioned between the oxygen atoms. In ice  $I_h$  each successive layer is a mirror image of the preceding layer, whereas in ice  $I_c$  each successive layer is in the same orientation but shifted by one half of the width of the puckered hexagonal ring. However, what is commonly observed through diffraction studies is, particularly at low temperatures, that ice I has a mixture of sequences associated with both ice  $I_c$  and ice  $I_h$ , i.e. it is stacking disordered.

Satellite based spectroscopic measurements indicate that mesospheric clouds are predominantly composed of crystalline ice, but cannot rule out a small fraction of cloud mass being comprised of amorphous ice (Hervig and Gordley, 2010). Murray and Jensen (2010) suggested that amorphous ice nucleates, since the amorphous phase has a lower energy barrier to nucleation than crystalline ice, but may subsequently crystallise. This would suggest that amorphous ice may be a transient phase in the upper mesosphere, which rapidly crystallises. Hervig and Gordley (2010) state that they cannot distinguish between the different forms of crystalline ice in mesospheric clouds, therefore the nature of

\* Corresponding author.

E-mail address: [BJ.Murray@Leeds.ac.uk](mailto:BJ.Murray@Leeds.ac.uk) (B.J. Murray).

mesospheric crystalline ice remains poorly constrained.

In this paper we report a sequence of experiments which show that crystalline ice grown at mesosphericly relevant conditions is a form of stacking disordered ice.

## 2. Methods

In order to determine the crystal structure of ice grown under conditions pertinent to the mesopause region, we examine ice grown on a temperature controlled stage enclosed within an environmental chamber using X-ray diffraction. In these experiments we deposited ice from the vapour phase onto a glass substrate at 110 K as amorphous ice and the sample was then warmed at a rate of  $1 \text{ K min}^{-1}$  while recording detailed diffraction patterns over a range of temperatures relevant for mesospheric clouds.

We have used X-ray diffraction to study vapour deposited ice (Shilling et al., 2006) and ice crystallised from aqueous solution droplets (Malkin et al., 2012; Murray, 2008a, 2008b; Murray and Bertram, 2006, 2007; Murray et al., 2005; Wagner et al., 2012) in the past. The X-ray diffractometer (Bruker D8 Advance) used in these experiments was configured in a standard reflection geometry and was equipped with a  $\text{Cu K}\alpha$  X-ray source ( $\lambda = 1.5418 \text{ \AA}$ ), a VANTEC detector and an Anton Paar TTK450 liquid nitrogen temperature-controlled stage. The stage is enclosed within an airtight chamber.

In order to prepare the ice film, the sample holder was cooled by liquid nitrogen to 110 K at a rate of  $30 \text{ K min}^{-1}$  with the chamber under vacuum. A diffraction pattern was taken to ensure no frosting had occurred during this process. If no detectable frosting of the sample support was detected, humidified nitrogen was admitted to the chamber. The pressure in the chamber was increased from  $1 \times 10^{-3}$  mbar to atmospheric pressure ( $\sim 1 \text{ atm}$ ) in approximately 5 min and the ice film was then left to grow for about 25 min after which an observable ice deposit was evident in the X-ray diffraction patterns. The water content of the nitrogen gas was controlled using a water bubbler and successive dilution using mass flow metres in order that the maximum saturation ratio (with respect to ice  $I_h$  and the cold stage set to 110 K) was about 12. Vapour deposition of ice in this manner is expected to result in a porous ice film made up of nano-scaled amorphous ice particles (Murray and Plane, 2003a, 2003b, 2005). Once deposition was complete, the chamber was placed under vacuum and diffraction patterns ( $2\theta = 10^\circ\text{--}60^\circ$ ) were recorded every 5 K as the sample was warmed continuously at  $1 \text{ K min}^{-1}$  from 110 K; warming the ice film in this way result in controlled and reproducible irreversible crystallisation.

## 3. Results and discussion

A sequence of diffraction patterns of ice which was initially deposited from the vapour phase at 110 K and then warmed at a rate of  $1 \text{ K min}^{-1}$ , together with the calculated ideal patterns of ice  $I_c$  and ice  $I_h$ , are shown in Fig. 1. The diffraction pattern of the ice which was initially deposited at 110 K has no sharp Bragg peaks, consistent with amorphous ice. The ice began to crystallise between 120 and 125 K as evidenced by the appearance of clear Bragg peaks. The intensity of the peaks in the patterns recorded between 125 and 160 K increase with increasing temperature as the amorphous ice crystallises. In the past, these patterns would have been identified as ice  $I_c$  on the basis that the three primary cubic peaks are present at  $24^\circ$ ,  $40^\circ$  and  $47.5^\circ$  in the experimental patterns. However, closer inspection reveals a number of inconsistencies: the respective intensities of the  $24^\circ$ ,  $40^\circ$  and  $47.5^\circ$  peaks are not a good match to the simulated pattern of ice  $I_c$ ; there is a

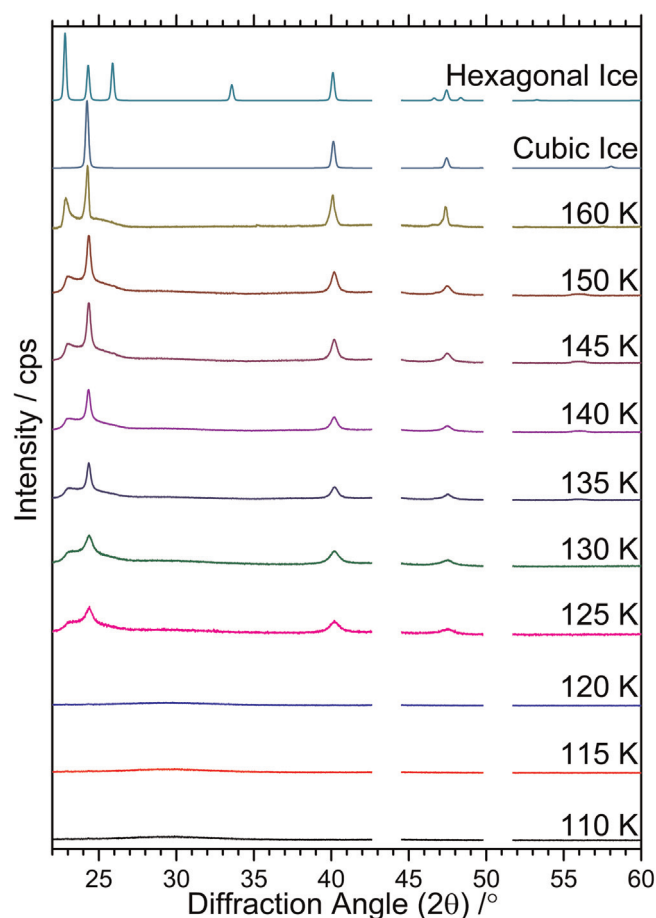


**Fig. 1.** X-ray diffraction patterns of deposited amorphous ice at 110 K (bottom), progressing to warmer temperatures (ascending patterns) with calculated pure ice  $I_c$  and pure ice  $I_h$  patterns at the top. The gaps in the pattern correspond to the positions of peaks from the cold stage. These patterns do not have the background subtracted. The Y axis is plotted as counts per second (cps).

peak at  $23^\circ$  at a position of a prominent peak in the simulated ice  $I_h$  pattern, but the absence of other ice  $I_h$  peaks ( $26^\circ$  and  $33.5^\circ$ ) shows that there is no bulk ice  $I_h$  present in the sample; finally, the region between  $23^\circ$  and  $26^\circ$  in the experimental patterns is raised above the background. In summary, the experimental patterns of crystalline ice over the mesospheric cloud temperature range are inconsistent with either ice  $I_h$  or ice  $I_c$ .

Instead, the features of these diffraction patterns are consistent with stacking disorder in ice I. In a study of the freezing of supercooled water droplets which froze around 233 K, showed that a diffraction pattern containing similar features was consistent with ice which had 50% cubic and 50% hexagonal sequences randomly arranged. The quantitative analysis was done using an algorithm for calculating diffraction patterns containing stacking disorder known as DIFFaX (Treacy et al., 1991). Subsequently we have used MCDIFFaX (Malkin et al., 2015; Salzmann, 2014) which incorporates the DIFFaX code in a Monte-Carlo based least square fitting routine which aids the analysis, especially in cases where stacking is complex.

MCDIFFaX can be used to model varying degrees of complexity of stacking disorder. In the simplest case, the probability of a particular layer appearing is independent of what came before. In this case we only need to define a single stacking probability,  $\Phi_c$  which indicates the probability of cubic stacking expressed as %. The probability of hexagonal stacking,  $\Phi_h$ , is simply  $100 - \Phi_c$  and the stacking in ice which follows this model is said to be random. This simple model is a good description for ice nucleated

homogeneously in supercooled water droplets (Malkin et al., 2012), but it has also been shown that ice generated in different ways has a more complex form of stacking (Hansen et al., 2008a, 2008b; Kuhs et al., 2012; Malkin et al., 2015).

The probability of finding a particular stacking sequence in ice can be influenced by the preceding sequences. This has the potential to cause significant complexity and is referred to as a memory effect. In the case where the nearest neighbour interactions influence stacking probability (1st order memory effects) we need to use two independent stacking probabilities,  $\Phi_{cc}$  and  $\Phi_{hc}$  which define the probabilities of cubic stacking after a previous cubic or hexagonal stacking events, respectively. The hexagonal stacking probabilities,  $\Phi_{ch}$  and  $\Phi_{hh}$ , are  $100 - \Phi_{cc}$  and  $100 - \Phi_{hc}$ , respectively. Kuhs et al. (2012) showed that 2nd order memory effects can also be important, that is, where the next nearest neighbour interactions play a role in stacking. In order to define these we need a model with four independent stacking probabilities ( $\Phi_{ccc}$ ,  $\Phi_{hcc}$ ,  $\Phi_{chc}$  and  $\Phi_{hhc}$ ). For a fuller description of memory effects and stacking probabilities see Malkin et al. (2015). In this paper we use MCDIFFaX with four stacking probabilities capable of describing second order memory effects.

The results of the fitting procedure using MCDIFFaX are listed in Table 1 and an example of a fit to a diffraction pattern, for ice at 130 K, is shown in Fig. 2. Comparison of the experimental diffraction pattern and the model fit in Fig. 2 shows that the model is capable of describing all of the non-cubic features of the diffraction pattern. The fitted stacking probabilities are  $\Phi_{ccc}=60.1\%$ ,  $\Phi_{hcc}=58.5\%$ ,  $\Phi_{chc}=65.1\%$  and  $\Phi_{hhc}=63.1\%$ . The good fit in Fig. 2 shows that the ice at 130 K which crystallised from amorphous ice is a form of ice  $I_{sd}$ .

A significant source of uncertainty in this analysis is the background subtraction of the diffraction pattern of the underlying support material from the diffraction pattern of ice. The uncertainty was estimated by repeating the background subtraction and model fit three times. The variability in resulting stacking probabilities was less than  $\pm 2.5\%$ .

Inspection of the stacking probabilities in Table 1 reveals that there is no significant second order memory in the stacking sequences in this ice. For example, if there were second order memory effects in this ice, we would expect significant differences between  $\Phi_{ccc}$  and  $\Phi_{hcc}$ , whereas they are equal within uncertainty. This means that the probability of a cubic sequence is not dependent on the identity of the next nearest sequence. The same applies for the pair  $\Phi_{chc}$  and  $\Phi_{hhc}$ . Hence, we also include in this table the equivalent first order memory  $\Phi_{hc}$  and  $\Phi_{cc}$  (details of the conversion are given by Malkin et al. (2015)). Again, the values for each pattern are identical within uncertainty indicating that there is no significant memory in the stacking sequences in this ice and that the stacking in the ice is approximately random. Hence, this ice is made up of between 50% and 63% cubic sequences randomly distributed amongst hexagonal sequences.

In order to illustrate the stacking probabilities derived here and

**Table 1**

The stacking ratios for Ice  $I_{sd}$  crystallised from amorphous ice determined using MCDIFFaX.

Temp. (K)	$\Phi_{ccc}:\Phi_{hcc}:\Phi_{chc}:\Phi_{hhc}$	$\chi^2$	$\Phi_{cc}:\Phi_{hc}$	Cubicity <sup>a</sup>
125	63.3:61.2:65.1:63.1	0.29	62.0:64.4	63.2
130	60.1:58.5:63.2:61.5	0.25	59.1:62.6	60.6
135	59.7:57.8:60.3:59.9	0.21	58.6:60.1	59.5
140	57.9:55.8:59.9:58.6	0.19	56.7:59.4	57.9
145	57.1:54.2:58.3:56.4	0.17	55.5:57.5	56.5
150	55.5:53.7:57.1:55.7	0.16	54.5:56.5	55.4
160	50.5:48.5:50.0:51.0	0.07	49.5:50.5	50.0

$$^a \text{Cubicity} = \frac{\Phi_{hc}}{\Phi_{hc} + (100 - \Phi_{cc})}$$

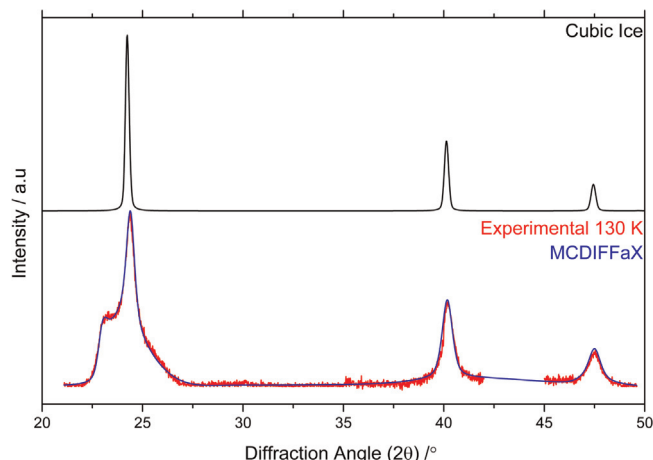


**Fig. 2.** Comparison of the experimental ice diffraction pattern recorded at 130 K with the MCDIFFaX model fit. The simulated pattern for well-defined ice  $I_c$  is also shown for comparison. Strong deviations from the ice  $I_c$  pattern are observed between  $2\theta=22^\circ$  and  $27^\circ$ , which are accounted for by the MCDIFFaX model where the stacking probabilities are listed in Table 1. This ice is clearly not ice  $I_c$ , but rather a stacking disordered ice, Ice  $I_{sd}$ .

compare them to stacking probabilities for ice made in different ways, we plot them in what we term a stackogram in Fig. 3. The literature data in this plot are taken from Malkin et al. (2015) and are compared with the new data for ice  $I_{sd}$  crystallised from amorphous ice.

The stackogram is a useful means of summarising  $\Phi_{hc}$  and  $\Phi_{cc}$  for various ices. The top right hand corner of the plot ( $\Phi_{hc}=100\%$  and  $\Phi_{cc}=100\%$ ) corresponds to well-defined ice  $I_c$ , whereas the bottom left corner ( $\Phi_{hc}=0\%$  and  $\Phi_{cc}=0\%$ ) corresponds to well-defined ice  $I_h$ . The top left corner ( $\Phi_{hc}=0\%$  and  $\Phi_{cc}=100\%$ ) corresponds to ice which is a mixture of bulk ice  $I_c$  and ice  $I_h$ , whereas the bottom right corner ( $\Phi_{hc}=100\%$  and  $\Phi_{cc}=0\%$ ) corresponds to ice where each cubic sequence is followed by a

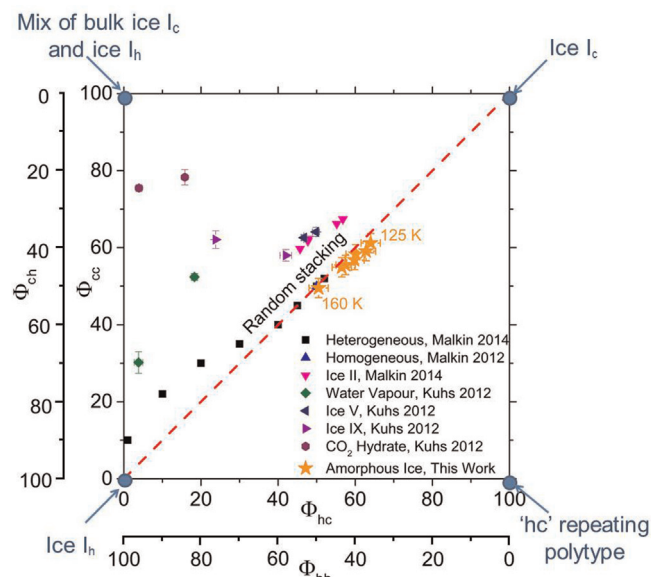


**Fig. 3.** A stackogram illustrating the stacking probabilities ( $\Phi_{hc}$  and  $\Phi_{cc}$ ) of ice I resulting from crystallisation of amorphous ice. We also show the compilation of literature data from Malkin et al. (2015). Specifically, the data includes stacking probabilities for ice from homogeneous nucleation in water (Malkin et al., 2012); heterogeneous nucleation in water and recrystallisation of ice II (Malkin et al., 2015); CO<sub>2</sub> hydrates and vapour deposition onto a cold substrate (Kuhs et al., 2012); and recrystallisation of ice V and IX (Hansen et al., 2008a, 2008b).

hexagonal sequence, and vice versa, creating an ordered polytype of ice I. The diagonal line represents the random line where  $\Phi_{hc} = \Phi_{cc}$ , i.e. where there is no memory in the stacking.

It is clear from Fig. 3 that ice  $I_{sd}$  which crystallised from amorphous ice is, within uncertainty, consistent with the random line (as mentioned above). It is also clear that the position on the random line is closer to well-defined ice  $I_c$  when it first crystallises at 125 K than the same sample once it has been warmed to 160 K and that the progression along the random line is systematic. At 160 K, the ice is close to the structure of ice resulting from the freezing of pure water droplets at 233 K (i.e.  $\Phi_{hc}=50\%$  and  $\Phi_{cc}=50\%$ ; Malkin et al., 2012). In contrast to the ice crystallised from amorphous ice or liquid water, ice  $I_{sd}$  generated from ice II (Malkin et al., 2015) and ice  $I_{sd}$  generated from other high pressure phases,  $CO_2$  hydrates and direct deposition (Kuhs et al., 2012) contains significant second order memory. Hence, the presence of memory in stacking disorder depends on the formation mechanism of ice  $I_{sd}$ .

In a computational study, Moore and Molinero (2011) found that cubic sequences outnumbered hexagonal ones by 2:1 (i.e. 67% cubic) in water which crystallised at around 180 K. The value for ice in our study at 125 K is 63% cubic. Crystal growth from amorphous ice is slow and progressed over an extended period of time as the sample was warmed; hence we were able to resolve some details of the transformation process. This means that we can observe the progression of crystallisation in these experiments and the results suggest that ice at the early stages of crystallisation tends to have a greater cubicity (proportion of cubic sequences).

#### 4. Conclusions

The results in this paper show that ice which crystallised at temperatures relevant for mesospheric clouds does not have a cubic crystal structure. Instead, it has a structure in which cubic and hexagonal sequences are randomly interlaced to produce stacking disordered ice. This has some consequences for our understanding of polar mesospheric clouds.

It has been suggested that large depolarisation ratios observed by lidar in mesospheric clouds can be explained by ice particles which adopt needle or column shapes (Baumgarten et al., 2002; Kokhanovsky, 2006; Rapp et al., 2007). These observations are at odds with the suggestion that ice in these clouds is made of ice  $I_c$ , since ice  $I_c$  is not expected to form needles. Ice  $I_c$  has a cubic crystal structure and is expected to form isotropic shapes, including cubes, octahedra or intermediate cubo-octahedra (Murray et al., in press; Whalley, 1981). Ice  $I_h$  on the other hand is expected to form strongly non-isotropic crystal shapes such as needles, columns and plates (Tape, 1994), but based on laboratory work it is not expected to form under mesospheric conditions (Murphy, 2003; Murray and Plane, 2005). While the depolarisation ratio data is inconsistent with the presence of ice  $I_c$  and mesospheric clouds are too cold for ice  $I_h$ , the depolarisation measurements may be consistent with the presence of ice  $I_{sd}$ .

Ice  $I_{sd}$  is in the trigonal crystal system (Hansen et al., 2008a, 2008b; Kuhs et al., 2012; Malkin et al., 2015; Murray et al., in press), and crystals of this ice can take on columnar, needle, or plate shapes which have three-fold symmetry when viewed from the basal face (Murray et al., in press). Hence, crystals of ice  $I_{sd}$  can have large aspect ratios, consistent with the lidar observations of Baumgarten et al. (2002). This may have implications for the retrieval of ice particle size and other cloud properties from remote sensing techniques (Kokhanovsky, 2006).

Ice  $I_{sd}$  can have a rougher surface than its hexagonal counterpart (Kuhs et al., 2012) and this could enhance reactive uptake of trace gases and also electron/ion attachment. It is also worth

noting that the ice made in previous studies of the uptake of atomic oxygen (Murray and Plane, 2003a, 2003b) and meteoric metals (Murray and Plane, 2005; Plane et al., 2004) was most likely ice  $I_{sd}$ , rather than ice  $I_c$ .

Since the local structures of ice  $I_{sd}$  and ice  $I_c$  are slightly different it would be expected that there are some spectroscopic differences between these ices. This was recently confirmed by (Carr et al., 2014) who compared the Raman spectra of different ice  $I_{sd}$  samples and ice  $I_h$ . Specifically, they showed subtle changes in peak positions, shapes and integrated areas in the coupled  $\nu(O-H)$  stretching region ( $\sim 2900\text{--}3800\text{ cm}^{-1}$ ) which correlated with the amount of stacking disorder in ice  $I_{sd}$ . Bertie and Jacobs (1977) also report differences in the IR between what they referred to as cubic and hexagonal ice in the  $20\text{--}240\text{ cm}^{-1}$  spectral range. This contrasts with the view expressed by Warren (1984) who concluded that the infrared spectra are 'practically identical'. The measured differences in spectra between ice  $I_{sd}$  and ice  $I_h$  opens the possibility that a suitable experiment could be designed to test for the presence of ice  $I_{sd}$  in clouds in the mesosphere and elsewhere in the atmosphere or even in the atmospheres of other planets.

Finally, ice  $I_{sd}$  is metastable with respect to ice  $I_h$  and this may have some consequences for mesospheric clouds. Shilling et al. (2006) experimentally determined that the specific ice  $I_{sd}$  they generated had a vapour pressure of  $11 \pm 3\%$  larger than that of ice  $I_h$  at 180–190 K; this corresponds to a difference in Gibbs free energy of  $155 \pm 30\text{ J mol}^{-1}$ . Based on Shilling et al.'s measurements, we estimate mesospheric ice  $I_{sd}$  to have a vapour pressure  $15 \pm 3\%$  larger than ice  $I_h$  at 130 K (Murray et al., 2010). In making this estimate we assume that the ice  $I_{sd}$  generated by Shilling et al. (2006) had a similar degree of stacking disorder to the ice we made here. This is a reasonable assumption since those authors also deposited amorphous ice and crystallised it by warming in a manner comparable to our procedure and their diffraction patterns have the distinct signature of stacking disorder. A greater equilibrium vapour pressure means that a cloud composed of ice  $I_{sd}$  would sublime at a lower temperature than a cloud made of ice  $I_h$ . Given the relatively small difference in vapour pressure we would expect this temperature difference to be only  $\sim 0.5\text{ K}$ .

While we have explored the structure of ice which crystallises from amorphous ice at mesospherically relevant temperatures more work is needed to fully explore the structure of ice which could form under mesospheric conditions. Specifically, it would be useful to compare the ice grown in the study with ice directly deposited at temperatures above 110 K. Above some, as yet, undefined temperature limit crystalline ice will be directly deposited onto the surface and this may be different to the ice crystallised from an amorphous precursor. In addition, deposition from vapour with extreme and variable saturation ratios should also be explored. It is feasible that the degree of stacking disorder (the cubicity and stacking probabilities) will vary with growth conditions. Nevertheless, in this paper we have clearly shown that ice which forms and exists under mesospherically relevant conditions is stacking disordered.

#### Acknowledgements

We thank the European Research Council (FP7, 240449 ICE), the Natural Environment Research Council (NE/I020059/1, NE/I013466/1, NE/K004417/1), the Royal Society (UF100144) and the Leverhulme Trust (RPG-2014-04) for funding.

#### References

- Baumgarten, G., Fricke, K.H., von Cossart, G., 2002. Investigation of the shape of noctilucent cloud particles by polarization lidar technique. *Geophys. Res. Lett.*

- 29 (13), 8-1–8-4.
- Bertie, J.E., Jacobs, S.M., 1977. Far-infrared absorption by ices Ih and Ic at 4.3 K and the powder diffraction pattern of ice Ic. *J. Phys. Chem.* 67 (6), 2445–2448.
- Carr, T.H.G., Shephard, J.J., Salzmänn, C.G., 2014. Spectroscopic signature of stacking disorder in ice I. *J. Phys. Chem. Lett.* 5 (14), 2469–2473.
- Hansen, T.C., Koza, M.M., Kuhs, W.F., 2008a. Formation and annealing of cubic ice: I. Modelling of stacking faults. *J. Phys. Condens. Matter* 20 (28).
- Hansen, T.C., Koza, M.M., Lindner, P., Kuhs, W.F., 2008b. Formation and annealing of cubic ice: II. Kinetic study. *J. Phys. Condens. Matter* 20 (28).
- Hervig, M.E., Gordley, L.L., 2010. Temperature, shape, and phase of mesospheric ice from solar occultation for ice experiment observations. *J. Geophys. Res.: Atmos.* 115 (D15), D15208.
- Hobbs, P.V., 1974. *Ice Physics*. Clarendon Press, Oxford.
- Jensen, E.J., Diskin, G., Lawson, R.P., Lance, S., Bui, T.P., Hlavka, D., McGill, M., Pfister, L., Toon, O.B., Gao, R., 2013. Ice nucleation and dehydration in the tropical tropopause layer. *Proc. Natl. Acad. Sci.* 110 (6), 2041–2046.
- Kokhanovsky, A.A., 2006. Modeling of light depolarization by cubic and hexagonal particles in noctilucent clouds. *Atmos. Res.* 79 (2), 175–181.
- Kuhs, W.F., Sippel, C., Falenty, A., Hansen, T.C., 2012. Extent and relevance of stacking disorder in “ice Ic”. *Proc. Natl. Acad. Sci.* 109 (52), 21259–21264.
- Loerting, T., Winkel, K., Seidl, M., Bauer, M., Mitterdorfer, C., Handle, P.H., Salzmänn, C.G., Mayer, E., Finney, J.L., Bowron, D.T., 2011. How many amorphous ices are there? *Phys. Chem. Chem. Phys.* 13 (19), 8783–8794.
- Lübken, F.J., Lautenbach, J., Höffner, J., Rapp, M., Zeche, M., 2009. First continuous temperature measurements within polar mesosphere summer echoes. *J. Atmos. Sol. Terr. Phys.* 71 (3–4), 453–463.
- Malkin, T.L.J.M.B., Salzmänn, C., Molinero, V., Pickering, S.J., Whale, T., 2015. Stacking disorder in ice I. *Phys. Chem. Chem. Phys.* 17 (1), 60–76.
- Malkin, T.L., Murray, B.J., Brukhno, A.V., Anwar, J., Salzmänn, C.G., 2012. Structure of ice crystallized from supercooled water. *Proc. Natl. Acad. Sci. U. S. A.* 109 (4), 1041–1045.
- Moore, E.B., Molinero, V., 2011. Is it cubic? Ice crystallization from deeply supercooled water. *Phys. Chem. Chem. Phys.* 13 (44), 20008–20016.
- Murphy, D.M., 2003. Dehydration in cold clouds is enhanced by a transition from cubic to hexagonal ice. *Geophys. Res. Lett.* 30 (23).
- Murray, B.J., 2008a. Enhanced formation of cubic ice in aqueous organic acid droplets. *Environmental Research Letters* 3 (2).
- Murray, B.J., 2008b. Inhibition of ice crystallisation in highly viscous aqueous organic acid droplets. *Atmos. Chem. Phys.* 8 (17), 5423–5433.
- Murray, B.J., Bertram, A.K., 2006. Formation and stability of cubic ice in water droplets. *Phys. Chem. Chem. Phys.* 8 (1), 186–192.
- Murray, B.J., Bertram, A.K., 2007. Strong dependence of cubic ice formation on droplet ammonium to sulfate ratio. *Geophys. Res. Lett.* 34 (16).
- Murray, B.J., Jensen, E.J., 2010. Homogeneous nucleation of amorphous solid water particles in the upper mesosphere. *J. Atmos. Sol. Terr. Phys.* 72 (1), 51–61.
- Murray, B.J., Broadley, S.L., Wilson, T.W., Bull, S.J., Wills, R.H., Christenson, H.K., Murray, E.J., 2010. Kinetics of the homogeneous freezing of water. *Physical Chemistry Chemical Physics* 12 (35), 10380–10387.
- Murray, B.J., Knopf, D.A., Bertram, A.K., 2005. The formation of cubic ice under conditions relevant to Earth’s atmosphere. *Nature* 434 (7030), 202–205.
- Murray, B.J., Plane, J.M.C., 2003a. Atomic oxygen depletion in the vicinity of noctilucent clouds. *Adv. Space. Res.* 31, 2075–2084.
- Murray, B.J., Plane, J.M.C., 2003b. The uptake of atomic oxygen on ice films: implications for noctilucent clouds. *Phys. Chem. Chem. Phys.* 5 (19), 4129–4138.
- Murray, B.J., Plane, J.M.C., 2005. Uptake of Fe, Na and K atoms on low-temperature ice: implications for metal atom scavenging in the vicinity of polar mesospheric clouds. *Phys. Chem. Chem. Phys.* 7 (23), 3970–3979.
- Murray, B.J., Salzmänn, C.G., Heymsfield, A.J., Dobbie, S., Neely-III, R.R., Cox, C.J. Trigonal ice crystals in Earth’s atmosphere. *Bulletin of the American Meteorological Society*, <http://dx.doi.org/10.1175/BAMS-D-13-00128.1>, in press.
- Palmer, J.C., Martelli, F., Liu, Y., Car, R., Panagiotopoulos, A.Z., Debenedetti, P.G., 2014. Metastable liquid–liquid transition in a molecular model of water. *Nature* 510 (7505), 385–388.
- Plane, J.M.C., Murray, B.J., Chu, X.Z., Gardner, C.S., 2004. Removal of meteoric iron on polar mesospheric clouds. *Science* 304 (5669), 426–428.
- Rapp, M., Thomas, G.E., Baumgarten, G., 2007. Spectral properties of mesospheric ice clouds: Evidence for nonspherical particles. *J. Geophys. Res. Atmos.* 112 (D3).
- Salzmänn, C.G., 2014. ([http://www.ucl.ac.uk/chemistry/research/group\\_pages/salzmänn\\_group](http://www.ucl.ac.uk/chemistry/research/group_pages/salzmänn_group)).
- Salzmänn, C.G., Radaelli, P.G., Slater, B., Finney, J.L., 2011. The polymorphism of ice: five unresolved questions. *Phys. Chem. Chem. Phys.* 13 (41), 18468–18480.
- Shilling, J.E., Tolbert, M.A., Toon, O.B., Jensen, E.J., Murray, B.J., Bertram, A.K., 2006. Measurements of the vapor pressure of cubic ice and their implications for atmospheric ice clouds. *Geophys. Res. Lett.* 33 (17).
- Tape, W., 1994. *Atmospheric Halos*. AGU, Washington, DC.
- Treacy, M.M.J., Newsam, J.M., Deem, M.W., 1991. A general recursion method for calculating diffracted intensities from crystals containing planar faults. *Proc. R. Soc. Lond. A* 433, 499–520.
- Wagner, R., Mohler, O., Saathoff, H., Schnaiter, M., Skrotzki, J., Leisner, T., Wilson, T.W., Malkin, T.L., Murray, B.J., 2012. Ice cloud processing of ultra-viscous/glassy aerosol particles leads to enhanced ice nucleation ability. *Atmos. Chem. Phys.* 12 (18), 8589–8610.
- Warren, S.G., 1984. Optical constants of ice from the ultraviolet to the microwave. *Appl. Opt.* 23, 1206–1225.
- Whalley, E., 1981. Scheiners halo-evidence for ice Ic in the atmosphere. *Science* 211 (4480), 389–390.
- Wilson, T.W., Murray, B.J., Wagner, R., Mohler, O., Saathoff, H., Schnaiter, M., Skrotzki, J., Price, H.C., Malkin, T.L., Dobbie, S., Al-Jumr, S., 2012. Glassy aerosols with a range of compositions nucleate ice heterogeneously at cirrus temperatures. *Atmos. Chem. Phys.* 12 (18), 8611–8632.